APL Materials

Electrically driven lasing in metal halide perovskites: Challenges and outlook

Cite as: APL Mater. 8, 030902 (2020); https://doi.org/10.1063/1.5143265
Submitted: 20 December 2019 . Accepted: 04 February 2020 . Published Online: 03 March 2020

William B. Gunnarsson, and Barry P. Rand

Electrically driven lasing in metal halide perovskites: Challenges and outlook

Cite as: APL Mater. 8, 030902 (2020); doi: 10.1063/1.5143265
Submitted: 20 December 2019 • Accepted: 4 February 2020 •
Published Online: 3 March 2020

William B. Gunnarsson[1] and Barry P. Rand[2,a)]

AFFILIATIONS

[1] Department of Electrical Engineering, Princeton University, Princeton, New Jersey 08544, USA
[2] Department of Electrical Engineering and Andlinger Center for Energy and the Environment, Princeton University, Princeton, New Jersey 08544, USA

Note: This paper is part of the Special Issue on Light Emission from Perovskite Materials.
[a)] **Author to whom correspondence should be addressed:** brand@princeton.edu

ABSTRACT

Metal halide perovskite semiconductors have shown great potential as emissive layers in light-emitting diodes and gain media in optically pumped lasers, and thus represent a possible foundation for a non-epitaxial electrically driven laser diode. However, degradation of perovskite-based devices and inability to maintain high-efficiency operation at large current densities have so far inhibited realization of this goal. This report will explore the causes underlying these observations—specifically, Joule heating, electric field-induced quenching, charge injection imbalance, and Auger recombination—and consider approaches to achieve an electrically driven perovskite laser diode.

I. INTRODUCTION

Metal halide perovskites are an emerging class of solution-processable semiconductors at the center of a rapidly growing research effort following their successful application as absorber layers in solar cells and emissive layers in light-emitting diodes (LEDs).[1–3] These materials exhibit excellent optoelectronic properties, including absorption coefficients of ~10^4 cm^{-1}, charge carrier mobilities exceeding 10 cm^2/V s, and trap densities less than 10^{16} cm^{-3} (Ref. 3), and have consequently come to the forefront of the effort to develop a non-epitaxial laser diode. A perovskite laser diode would potentially offer a low-cost, easily fabricated, and wavelength-tunable coherent optical source which could be incorporated in flexible and lightweight devices. However, major obstacles remain on the path to electrically pumped lasing in perovskites.

A variety of perovskite formulations have exhibited lasing under short-pulse optical excitation at room temperature.[4,5] This was first achieved in 2014 using a layer of $MAPbI_{3-x}Cl_x$ (MA = methylammonium, $CH_3NH_3^+$) in a vertical cavity structure between a gold layer and a dielectric mirror.[6] In recent years, perovskite lasers have been developed using both single crystals and polycrystalline films in several resonator geometries, including whispering gallery mode microspheres[7,8] and nanoplatelets,[9] Fabry–Perot mode nanowires,[10] and thin films with embedded photonic structures such as etched or stamped distributed feedback (DFB) gratings.[11–14] Recently, optically pumped lasing has even been demonstrated in complete and operational perovskite LED structures with embedded DFB resonators.[15]

An important step toward the ultimate goal of an electrically driven perovskite laser diode is demonstration of continuous-wave (CW) optically pumped amplified spontaneous emission (ASE) and lasing. Initial investigations found that lasing in a $MAPbI_3$ thin film ceased after ~25 ns under continuous excitation at 160 K, due primarily to pump-induced heating and consequent threshold increase.[12,16] More recently, CW lasing has been demonstrated in $MAPbI_3$ at a temperature of ~100 K (Ref. 17), and CW ASE has been observed at 120 K in a phase-stable mixed-cation perovskite film.[18]

Electrically driven injection of electrons and holes into the perovskite active layer is another requirement for a laser diode, and is readily achieved using an LED structure. Typical LED configurations comprise a perovskite emissive layer, organic electron and hole transport layers (ETL and HTL), a metal top electrode, and a transparent conducting oxide bottom electrode through which light is emitted (see Refs. 3 and 19 for detailed discussions of

perovskite LED structures). Perovskite LEDs have recently surpassed 20% external quantum efficiency (EQE),[20–23] owing largely to incorporation of organic species into the perovskite precursor solution, which tends to shrink and passivate grains and allows for smooth, pinhole-free films. For instance, incorporation of *n*-butylammonium halides into $MAPbI_3$ and $MAPbBr_3$ precursors enhanced LED EQE from 1.0% to 10.4% and 0.03% to 9.3%, respectively.[24] Similarly, Lin *et al.* observed a >50× efficiency improvement in $CsPbBr_3$-based LEDs by addition of MABr, which formed a passivating shell around $CsPbBr_3$ perovskite grains to improve luminous efficiency.[20] Furthermore, addition of appropriately selected bulky ligands can induce 2-dimensional perovskite quantum wells, with thickness varying from one to several monolayers, forming a structure termed quasi-2D or mixed 2D/3D perovskite. Highly luminescent films and efficient LEDs have been fabricated using quasi-2D perovskites, often attributed to funneling of charge carriers to regions of widest quantum wells and, thus, smallest bandgap.[25] These advances in perovskite LEDs and optically pumped lasers have paved the way toward development of an electrically driven laser diode.

II. PRIMARY CHALLENGES IN THE DEVELOPMENT OF A PEROVSKITE LASER DIODE

The progression from LED to laser diode will require (i) incorporation of an optical feedback structure, most likely a lithographically defined photonic structure etched or stamped into one of the device layers, and (ii) injection of a very large density of charge carriers while avoiding emission-quenching processes. An estimate of the requisite EQE–current density (J) product to achieve lasing in an LED-style perovskite laser diode is 62 A/cm^2, based on a threshold carrier density $n_{th} \sim 8 \times 10^{17}$ cm^{-3} measured in a $MAPbI_3$ film on a metal-clad distributed feedback grating.[12,26] It follows that the threshold current density would be at least several hundred A/cm^2, depending on the ability to maintain a substantial EQE at high current densities. While perovskite LEDs have demonstrated EQEs greater than 20%, the EQE typically peaks at $J < 100$ mA/cm^2 and decreases severely at higher currents, a phenomenon termed EQE roll-off.[27,28] While the precise cause of roll-off is often difficult to pinpoint, Ohmic/Joule heating, charge carrier imbalance, electric fields in the emissive region, and Auger recombination have been proposed to play a role in the process.

An additional obstacle to achieving laser operation under electrical pumping is the permanent device degradation that occurs in perovskite LEDs after minutes to hours of continuous operation.[3] The rate of degradation is strongly dependent on the current density and other operating conditions, and, like EQE roll-off, can be influenced by several mechanisms. High current densities induce the fastest device failure, though even relatively low current densities [e.g., 3 mA/cm^2 (Ref. 29)] will permanently worsen LED performance over time.

Successful development of a perovskite laser diode will depend on the ability to alleviate both EQE roll-off and device degradation, as the former determines the threshold current density and the latter determines whether the device can withstand such intense excitation. The subsequent sections will address potential causes of roll-off and degradation and will discuss strategies to mitigate these.

A. Thermal effects due to Joule heating

The operating temperature of a perovskite laser diode will require careful management. Even at relatively low current densities, Joule heating has proven to be significant in perovskite LEDs, as shown by the gradual evolution of the electroluminescence (EL) spectrum of an LED operating continuously at 40 mA/cm^2 for 70 s [Fig. 1(a)].[30] Based on the broadening of the high-energy tail of the spectrum, Zhao *et al.* determined that the carrier temperature in the perovskite layer increased from 24 °C to 41 °C over this time period. Similar behavior has been observed using a thermocouple probe attached to the cathode of an operating perovskite LED as well as infrared thermal imaging.[30,31] Given that the power dissipated as heat in an operating LED scales with I^2R, where I gives the total current and R gives the resistance of the device, one can expect this increase in temperature to become much more severe at current densities relevant to lasing.

Even a few tens of °C can substantially impact EQE and device lifetime. For instance, Shi *et al.* studied the temperature dependence of EL from a perovskite LED with a $CsPbBr_3$ quantum dot (QD) active layer over a range of temperatures relevant to Joule heating, maintaining a fixed current density of 50 mA/cm^2 (Ref. 32). It was found that the total emission intensity was reduced by over 30% in the first 23 °C above room temperature, and emission was almost entirely quenched around 93 °C above room temperature, as illustrated in Fig. 1(b). This heat-induced reduction in EL is consistent with time-resolved photoluminescence (TRPL) investigations of the monomolecular recombination rate in $MAPbI_3$ by Milot *et al.*, which show that the trap-mediated recombination increases sharply with temperature above 300 K [Fig. 1(c)].[33] The authors propose that this effect is due to thermal ionization of impurities in $MAPbI_3$, causing an increased density of trapping sites with increased temperature. However, Shi *et al.* noted that the photoluminescence (PL) of bare $CsPbBr_3$ QD films showed less severe thermal quenching than the EL of full LEDs, suggesting a mechanism more complex than can be explained solely by a thermally induced change in non-radiative rate.[32]

Zhao *et al.* examined the effect of temperature on operational stability by tracking the EQE of a $MAPbI_3$-based LED at a constant current density of 10 mA/cm^2 at various temperatures.[30] As shown in Fig. 2(a), the time required for the EQE to decrease to 80% of its initial value increased by a factor of ~40 when environmental temperature was reduced from 40 °C to 10 °C. However, the authors note that annealing a full device at 50 °C for 5 h did not impact the EQE, leading to the conclusion that the device degradation observed during operation is induced not by heat alone, but instead by a highly temperature-dependent process driven by electrical stress. To understand the mechanism behind this process, we consider the EQE enhancement observed by Zhao *et al.* when perovskite LEDs were voltage-cycled several times. The authors found that this enhancement was significant at room temperature (300 K) but ceased to occur below 220 K [see Fig. 2(b)].[29] This closely follows the observed temperature dependence of hysteresis in perovskite solar cells,[34] which has been studied intensively and attributed to mobile ionic species in the perovskite layer.[35] Collectively these studies suggest that heat-induced EQE roll-off and device degradation may be related to the movement of ionic species under an applied

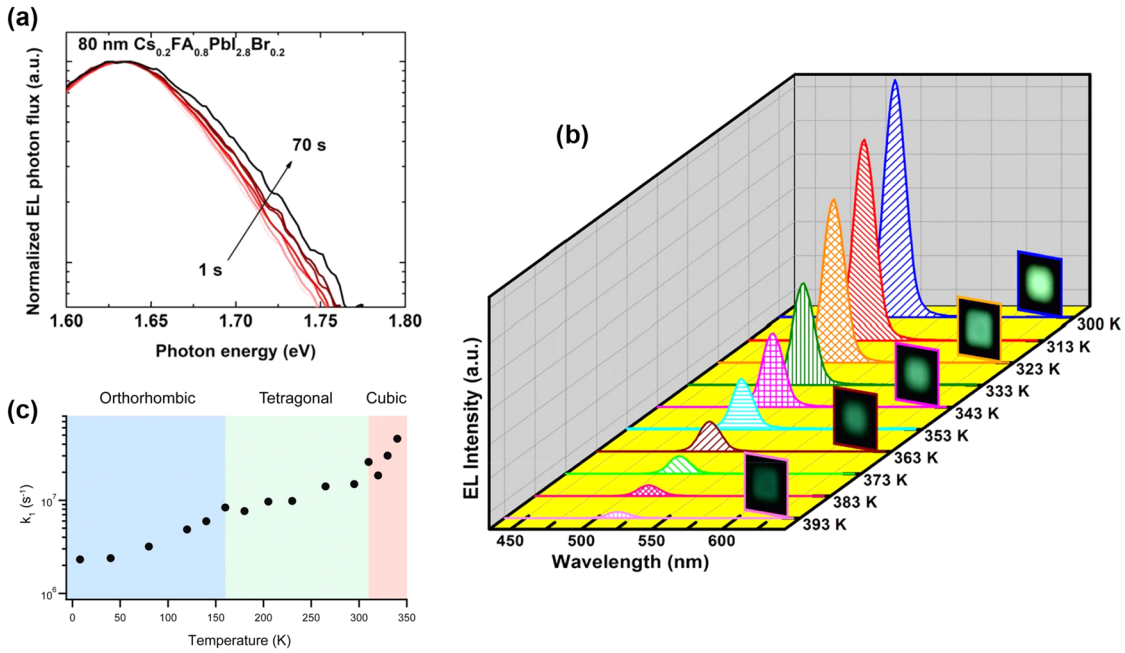

FIG. 1. (a) Evolution of the high-energy region of the EL spectrum of a perovskite LED under a constant current of 40 mA/cm^2 over 70 s. Reproduced with permission from Zhao *et al.*, Adv. Mater. **31**, 1805836 (2019). Copyright 2019 Wiley-VCH. (b) Temperature-dependent EL spectra and photographs of a $CsPbBr_3$ QD LED operating at a fixed current density of 50 mA/cm^2. Reprinted with permission from Shi *et al.*, ACS Nano **12**, 1462 (2018). Copyright 2018 American Chemical Society. (c) Monomolecular recombination rate (k_1) in $MAPbI_3$ measured by TRPL at various temperatures. Reproduced with permission from Milot *et al.*, Adv. Funct. Mater. **25**, 6218 (2015). Copyright 2015 Wiley-VCH.

electric field, which may lead to reactions at interfaces and create defects sufficient to quench emission.

The optical gain in a perovskite laser diode will also be impacted severely by heating of the active layer. Figure 2(c) shows the ASE threshold in a perovskite thin film under pulsed optical excitation between 80 K and 290 K, which reveals an increase in threshold with temperature that appears to accelerate exponentially, particularly near room temperature.[18] This trend results from a combination of increased non-radiative recombination and spreading of the energetic distribution of carriers in the conduction and valence bands at higher temperature, making population inversion more difficult to achieve. Indeed, an exponential relationship between the threshold current and temperature is typical of epitaxially grown semiconductor laser diodes for the same reasons.[36]

Multiple options are available to combat the effects of Joule heating, all of which likely must be applied if electrically pumped lasing is to be achieved in metal halide perovskites. The first of these strategies is reduction of the environmental temperature. In a laboratory setting, this can be accomplished by allowing the device to operate in a cryostat, while in an applied setting, the device substrate might be cooled by Peltier cooling or a similar scheme. Cooling the device during operation will not prevent Joule heating (and could in fact exacerbate it due to the thermal dependence of carrier mobilities in commonly used organic charge transport layers), but the operating temperature of the device will be reduced by the same amount as the environmental temperature. The remaining strategies seek to reduce temperature by improving dissipation of heat from the active region of the device. Perovskites are known to have very low thermal conductivities (~0.5 W/m K in $MAPbI_3$ at room temperature[37,38]), making heat dissipation both challenging and vital. The primary approaches to maximize heat dissipation are reduction of the device area, use of short-pulse electrical excitation, and selection of high-thermal conductivity substrates and device layers. While there are few reports examining heat dissipation in perovskite devices under high current density, these techniques have been tested and their effectiveness proven using organic semiconductor films, which suffer from similarly low thermal conductivites (~0.2–0.5 W/m K in typical organic semiconductors[39]). For instance, Kasemann *et al.* showed that the breakdown current density of a 100 nm-thick doped organic film could be increased from 230 A/cm^2 to 6.2 kA/cm^2 by reducing the width of the driving electrical pulses from 5 μs to 50 ns (Ref. 40). Matsushima *et al.* used a lithographically defined active region to reduce the area of a copper phthalocyanine device from 625 μm^2 to 7.9 μm^2, and consequently increased the breakdown DC current density from 574 A/cm^2 to 128 kA/cm^2 (Ref. 41). Nakanotani *et al.* examined the effect of substrate thermal conductivity and found that by varying the substrate from glass (1 W/m K) to sapphire (46 W/m K) or silicon (148 W/m K), the breakdown current in an organic film could be increased from 567 to 823 and 1167 A/cm^2, respectively.[42]

Xu *et al.* investigated the impact of some of these measures on EQE roll-off in a perovskite LED operating at relatively high

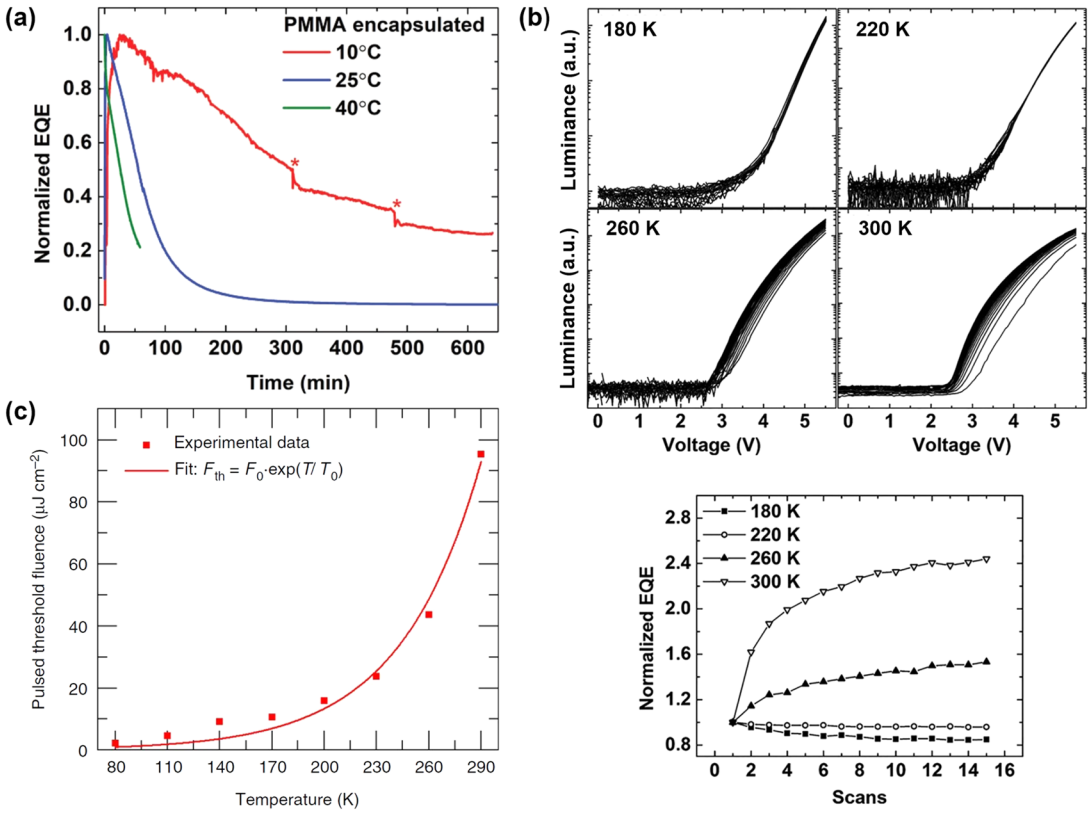

FIG. 2. (a) Operational stability of $MAPbI_3$ LEDs at various temperatures under a constant current density of 10 mA/cm^2 (asterisks mark times at which cryostat was refilled with liquid N_2). Reproduced with permission from Zhao *et al.*, Adv. Mater. **31**, 1805836 (2019). Copyright 2019 Wiley-VCH. (b) Luminance of a $MAPbI_3$ LED during repeated voltage scans at four different temperatures, and (below) the maximum EQE during each scan at each temperature (normalized to that of the first scan). Reproduced with permission from Zhao *et al.*, Adv. Mater. **29**, 1605317 (2017). Copyright 2017 Wiley-VCH. (c) ASE threshold in a perovskite film under pulsed optical excitation measured at various temperatures. Reproduced with permission from Brenner *et al.*, Nat. Commun. **10**, 988 (2019). Copyright 2019 Springer Nature.

current densities up to 80 A/cm^2 (Ref. 43). Figures 3(a) and 3(b) reveal the impact of reducing either excitation pulse width or environmental temperature on EL yield at high current density. By reducing the pulse duty cycle from 1% to 0.1%, the authors were able to enhance the maximum EL by over 50%, a similar effect to that seen when the environmental temperature was reduced from 300 K to 185 K. Furthermore, reducing the environmental temperature to 77 K led to a factor of 4 increase in maximum EL relative to 300 K operation, though the benefits of reduced temperature appear to saturate around this point, as 6 K resulted in roll-off at lower current density and reduced maximum EL. The authors propose that this may be due to Auger recombination, though charge imbalance and other effects may also be at play, and will be discussed further in Sec. II D.

To realize the full utility of pulsed operation at high current density, electrical pulses must be separated by enough time to allow for excess heat to dissipate completely and the pulse width must be minimized, as Joule heating can generate a substantial temperature increase on the sub-μs time scale. Kim *et al.* elucidated the latter requirement while examining a lithographically defined $MAPbI_3$ LED with 200 μm diameter operated under 2 μs electrical pulses (near the minimum achievable pulse width due to parasitic capacitance in the device architecture).[26] The authors recorded EL spectra under pulsed current densities up to 203 A/cm^2 [shown in Fig. 3(c)], revealing substantial heating of the active layer as evidenced by broadening of the high-energy side of the spectrum. At 203 A/cm^2, the temperature of the active region was estimated to have increased by over 50 °C during a 2 μs current pulse, corroborated by finite element thermal modeling shown in Fig. 3(d). The computed transient temperature increase, shown in the inset of Fig. 3(d), suggests that heating occurs fastest in the first few hundred ns. Interestingly, the observed EL intensity transient, when inverted and scaled by a constant factor [shown as dots in the inset of Fig. 3(d)], very closely follows the computed temperature increase, suggesting an intimate connection between the two effects. These results highlight the importance of ultra-short electrical pulses, which necessitate short rise times and hence require elimination of capacitance in the device architecture and driving circuit. This is an engineering challenge, but does not represent a fundamental obstacle in developing a perovskite laser diode.

Researchers have just begun to access the high current density regime in perovskite LEDs by reducing device size and electrical

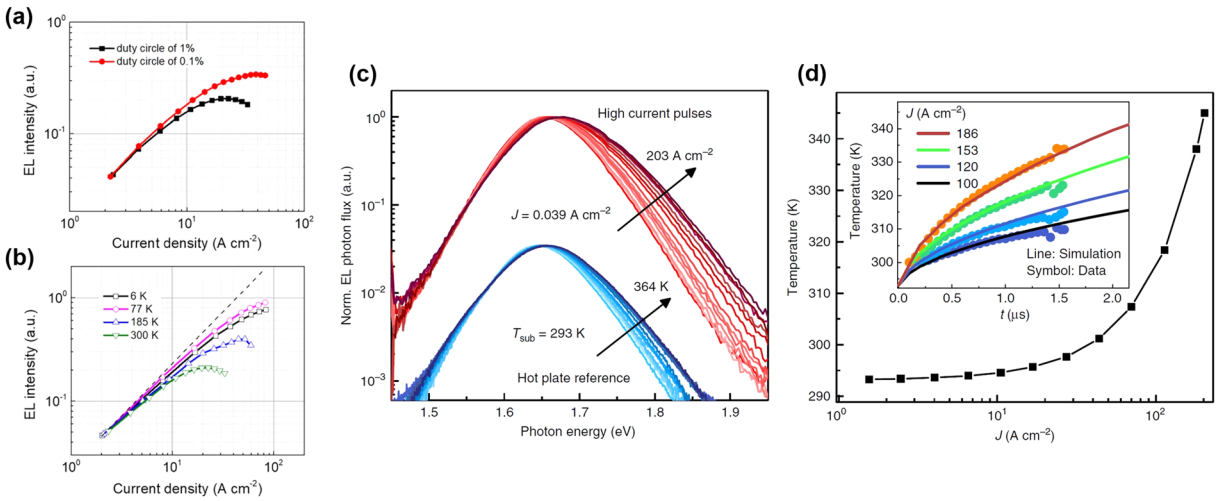

FIG. 3. EL intensity vs current density for a quasi-2D perovskite LED operating at varied (a) pulse duty cycle and (b) temperature. Reproduced with permission from Xu *et al.*, Appl. Phys. Lett. **115**, 041102 (2019). Copyright 2019 AIP Publishing LLC. (c) EL spectra of a $MAPbI_3$ LED under varied pulsed current density (red traces). Blue traces show EL spectra under J = 1 mA/cm^2 DC at varied temperature as a reference. (d) Finite element simulation of the temperature of the $MAPbI_3$ layer at the end of a 2 μs pulse with varied current density. The inset shows computed temperature transient (solid lines) at different current densities. Overlaid data points show the transient EL intensity inverted and scaled by a constant factor to underscore the relationship between EL and temperature. Reproduced with permission from Kim *et al.*, Nat. Commun. **9**, 4893 (2018). Copyright 2018 Springer Nature.

pulse width. Future work must incorporate high-thermal conductivity materials and leverage external cooling schemes if the $J > 1$ kA/cm^2 regime is to be reached with reasonable luminescent efficiency. This will introduce another challenge as the organic charge transport layers typically used in perovskite LEDs become much more resistive at low temperatures, and thus, the standard perovskite LED structure may need to be adjusted.

B. Electric field-induced quenching

Several reports have shown evidence that the presence of an electric field in the active layer of a perovskite LED can quench luminescence and may contribute to efficiency roll-off. While the cause of this phenomenon has not been carefully investigated, researchers speculate that the electric field may sweep electrons and holes apart and thereby reduce the probability of recombination. Perovskite emissive layers may experience electric fields on the order of 10^7 V/m, given device thicknesses and applied voltages on the order of 100 nm and a few volts, respectively. This estimate is of course complicated by large variations in conductivity throughout different device layers as well as non-Ohmic interfaces, but, nevertheless, serves as a rough approximation.

Zou *et al.* probed the effect of electric field on an LED with a quasi-2D perovskite emissive layer by measuring the PL quantum efficiency (PLQE) of the perovskite layer while a voltage bias was applied to the device [Fig. 4(a)].[44] The PLQE reaches a local maximum at 0.75 V and falls off symmetrically with voltage bias in either direction. The authors propose that the 0.75 V bias provides a flat band condition in the perovskite emissive layer (i.e., the applied bias offsets fields in the recombination zone originating from regions of built-in space charge), and thus, the symmetrical PLQE roll-off in either direction results from the electric field experienced by the photogenerated charge carriers. Above 1.5 V, the PLQE is enhanced via trap filling by electrically injected carriers before rolling off with the EQE due to effects discussed in Sec. II D. Below 0.75 V, the PLQE decreases continuously as the voltage bias becomes more negative, which, in the absence of a substantial population of injected carriers or Joule heating from electrical current, is likely attributable to the electric field. TRPL measurements [Fig. 4(b)] show that the PL lifetime also decreases as the voltage bias is varied from 0.75 V to −2 V. The proposed explanation for the observed quenching is that the electric field sweeps carriers in the emissive region apart and toward interfaces which typically contain a greater density of deep traps. This mechanism is supported by the phenomenon illustrated in Fig. 4(c), which shows EL from a quasi-2D perovskite LED during 10 μs electrical pulses.[45] A sharp ~1 μs spike in EL intensity directly follows the end of the pulse, suggesting that spatially separated electron and hole populations may build up during the pulse, held there by the applied electric field, then recombine when the applied field is turned off.

Electric field-induced quenching can also be impacted by ionic processes that occur within the perovskite active layer during LED operation. Kim *et al.* performed electroabsorption measurements on a $MAPbI_3$ LED to probe the transient behavior of the electric field in the perovskite layer while the applied bias was switched between −2 V and 2 V [Ref. 26]. As shown in Fig. 5(a), the applied field was screened on a timescale of about 0.5 s, consistent with rates previously observed for ionic processes in perovskite.[46] This suggests that an LED operating under short electrical pulses could be influenced by a DC bias which would redistribute charged mobile species in the perovskite layer and thereby alter the field distribution. Indeed, Fig. 5(b) shows that the PL lifetime in the $MAPbI_3$ layer of an LED measured during a 50 mA/cm^2 electrical pulse is reduced relative

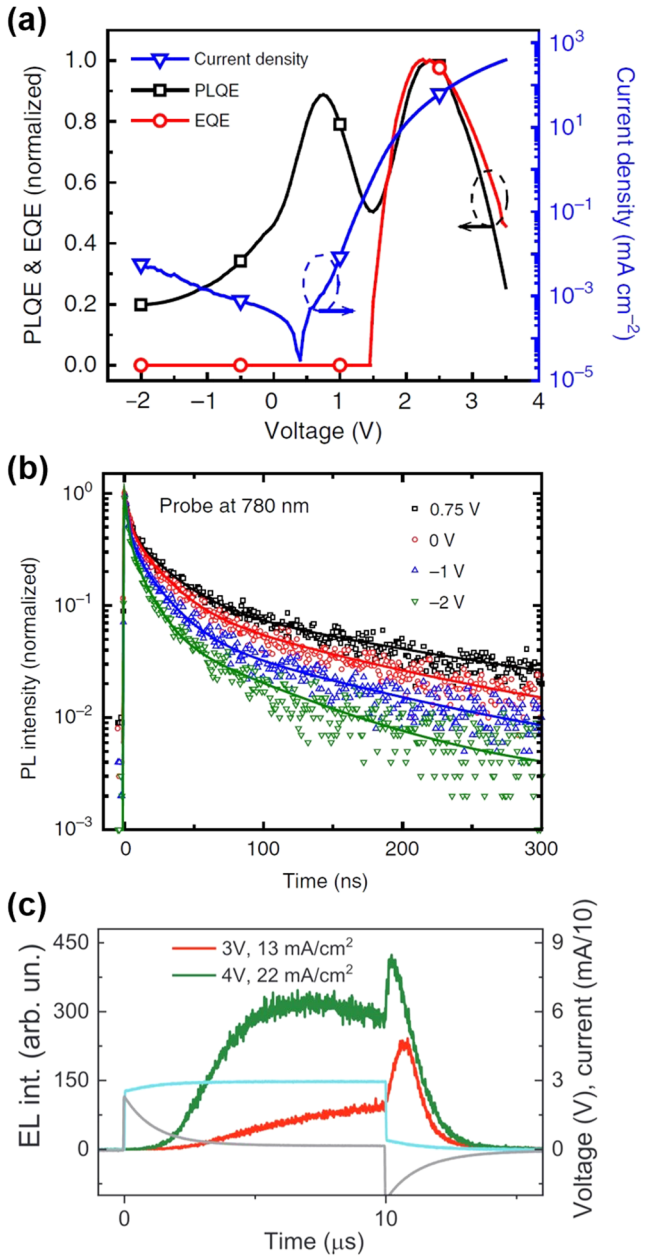

FIG. 4. (a) Dependence of the current density, EQE, and PLQE on driving voltage in a quasi-2D perovskite LED. (b) Transient PL decays measured in a quasi-2D perovskite LED under different bias conditions. Reproduced with permission from Zou *et al.*, Nat. Commun. **9**, 608 (2018). Copyright 2018 Springer Nature. (c) EL (green, red), voltage (blue), and current (gray) in a quasi-2D perovskite LED during a 10 μs electrical pulse, exhibiting a large EL overshoot following the end of the pulse. Reproduced with permission from Fakharuddin *et al.*, Adv. Funct. Mater. **29**, 1904101 (2019). Copyright 2019 Wiley-VCH.

to that measured 1 μs before the electrical pulse *unless* a 2.5 V DC bias is present. Furthermore, a 3 V background bias produced a ~3× increase in EQE at J = 10 A/cm^2 (as compared to the case with 0 V background bias).[26]

The electric field in the perovskite layer can also have a pronounced effect on optical gain and, thus, will be relevant in a perovskite laser diode. Yuan *et al.* measured ASE from a $MAPbI_3$ film sandwiched between thick insulating polymer layers then conductive contacts, allowing application of an electric field without current injection.[47] Figure 5(c) shows the total spontaneous emission (SE) and ASE intensities as a function of the estimated electric field in the $MAPbI_3$ layer, with the change in emission profile shown in Fig. 5(d). The authors find that ASE under a constant pump intensity of 97 μJ/cm^2 is completely eliminated by an applied bias of 25 V, corresponding to an approximate electric field of 3.3×10^5 V/cm.

The impact of field-induced quenching on EQE at very large current densities (J > 100 A/cm^2) is difficult to determine. It is possible that a sufficient population of injected carriers would easily screen the electric field in the bulk of the emissive material and thereby reduce its impact on radiative recombination probability. However, the EQE enhancement observed by Kim *et al.* due to a 3 V DC background bias during pulsed operation persisted up to tens of A/cm^2, indicating that field-induced quenching remains significant at these current densities.[26] Moreover, the aforementioned screening effect would create strong fields localized at the perovskite-transport layer interfaces, which could introduce additional degradation pathways through, for example, field-driven deprotonation of organic cations in the perovskite.[48]

C. Charge carrier injection imbalance

Maintaining balanced injection of electrons and holes into the emissive layer has proven to be important in achieving high EQE in perovskite LEDs.[49,50] This is accomplished primarily through selection of appropriate charge transport layers. An ETL with a large ionization energy and HTL with a small electron affinity will provide energy barriers that prevent injected charge carriers from leaking out of the emissive layer into the transport layers and thereby reducing EQE. Even with excellent charge blocking, however, charge carrier imbalance can be problematic if one type of charge carrier is injected more efficiently than the other due to a difference in injection barriers or transport layer conductivities for electrons and holes. If, for instance, electrons are injected more efficiently, they will pass through the emissive layer and build up at the HTL interface. The resulting efficiency will likely be poor relative to the case where the recombination zone is in the bulk of the emissive material as interfaces tend to have higher trap densities, inducing non-radiative recombination.

While balanced charge injection is clearly needed to achieve a high EQE, it is not obvious how charge imbalance may affect EQE roll-off or device degradation. Fakharuddin *et al.* investigated these effects in an LED with a quasi-2D perovskite emissive layer, 4,7-diphenyl-1,10-phenanthroline (BPhen) ETL, and poly(4-butylphenyl-diphenyl-amine) (polyTPD) HTL.[45] Because the electron conductivity of BPhen is ~5 times greater than the hole conductivity of polyTPD, the recombination zone is located at the perovskite–polyTPD interface. By doping the BPhen ETL with 10% Alq_3 [tris(8-hydroxy-quinolinato)aluminum], its electron conductivity can be reduced to a level similar to the hole conductivity of polyTPD, confirmed by J–V curves measured for electron- and

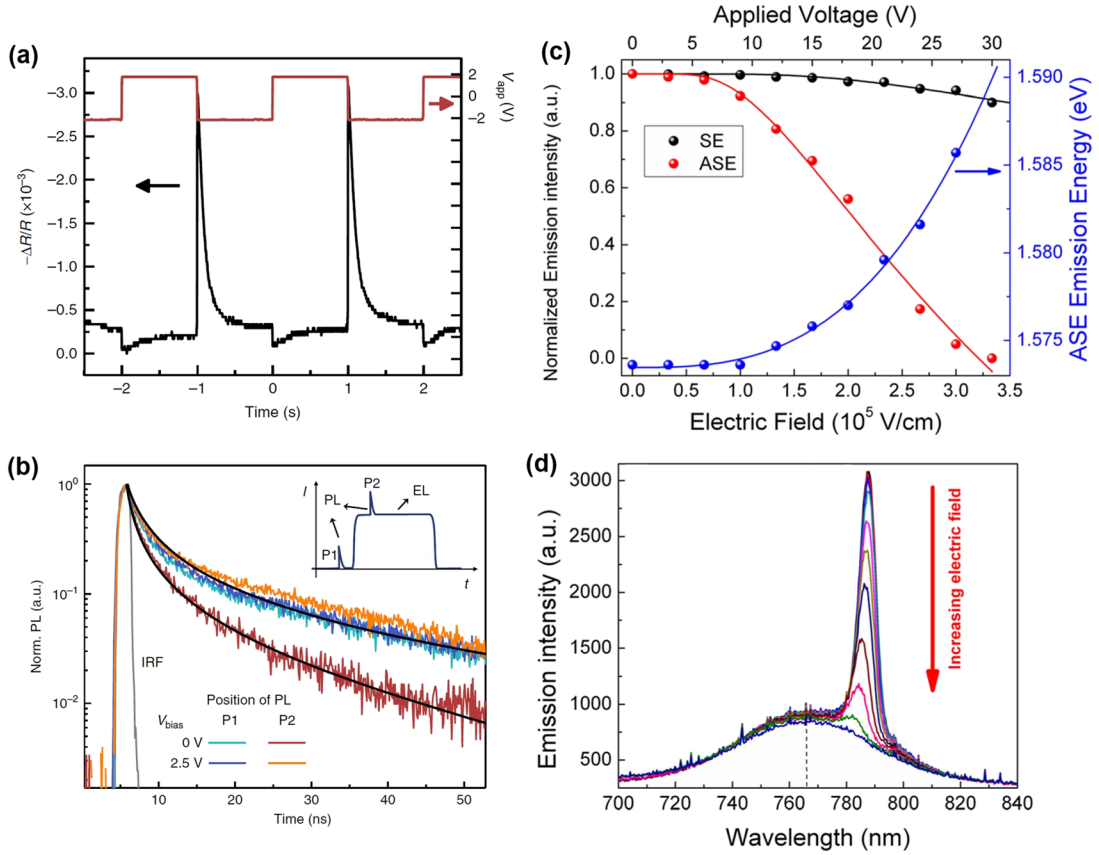

FIG. 5. (a) Time-dependent electroabsorption signal of a $MAPbI_3$ LED (black, measured via the reflectivity response of a 730 nm probe beam to a small voltage oscillation) as a square wave in voltage is applied to the device (red), revealing a slow screening of the electric field in the perovskite layer. (b) TRPL decays recorded in a $MAPbI_3$ LED 1 μs before (P1) and after (P2) the onset of a 50 mA/cm^2 electrical pulse, with a background DC voltage bias of 0 V or 2.5 V (see legend in figure). Reproduced with permission from Kim *et al.*, Nat. Commun. **9**, 4893 (2018). Copyright 2018 Springer Nature. (c) Electric field dependence of SE (black) and ASE (red) intensity and ASE peak emission energy (blue) from $MAPbI_3$ under 97 μJ/cm^2 excitation intensity. (d) Evolution of the emission spectrum as the applied DC voltage bias increases, illustrating quenching of ASE. Adapted with permission from Yuan *et al.*, Appl. Phys. Lett. **107**, 261106 (2015). Copyright 2015 AIP Publishing LLC.

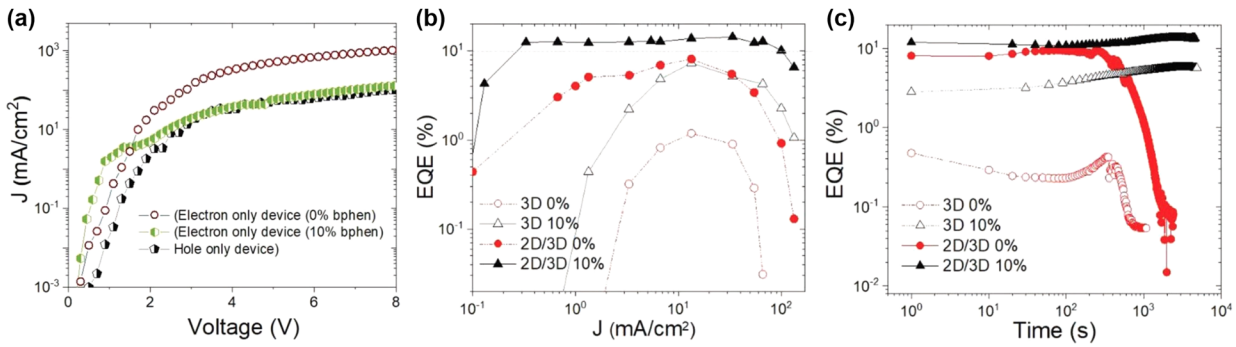

FIG. 6. (a) *J–V* measurements of single-carrier devices (hole-only: polyTPD/perovskite/polyTPD, electron-only: ZnO/PEIE/perovskite/BPhen with BPhen doped by 0% or 10% Alq_3), indicating more balanced injection capabilities of the HTL and ETL following addition of Alq_3. (b) EQE roll-off and (c) operational stability (J = 13 mA/cm^2) of LEDs with either 3D (hollow symbols) or quasi-2D (filled symbols) perovskite emissive layers and BPhen ETLs doped by 0% (red) or 10% (black) Alq_3. Reproduced with permission from Fakharuddin *et al.*, Adv. Funct. Mater. **29**, 1904101 (2019). Copyright 2019 Wiley-VCH.

hole-only devices, shown in Fig. 6(a). The quasi-2D perovskite LEDs with Alq_3-doped BPhen show a peak EQE of 13.8%, improved from 8.1% with pristine BPhen, and maintain an EQE of 10.8% at 100 mA/cm^2 and 4.1% at 200 mA/cm^2, while the device with pristine BPhen rolls off to 0.9% EQE at 100 mA/cm^2 and degrades at 200 mA/cm^2 [see 2D/3D plots in Fig. 6(b)].

Figure 6(c) reveals that while devices with pristine BPhen begin to degrade after a few minutes under J = 13 mA/cm^2, devices with Alq_3-doped BPhen show no degradation after 90 min. Moreover, the authors report device lifetimes improved by a factor of ~50 for various current densities between 10 mA/cm^2 and 100 mA/cm^2. Figures 6(b) and 6(c) show similar results obtained for LEDs with pure 3D perovskite. Furthermore, the authors observe that when the polyTPD HTL is doped with F_6TCNNQ [2,2'-(perfluoronaphthalene-2,6-diylidene)dimalononitrile], increasing its hole conductivity, devices with pristine BPhen ETL display improved performance as compared to those with Alq_3-doped BPhen, confirming that the observed effects are due to improved charge balance.

D. Auger recombination

At the high current densities required for electrically pumped lasing in an LED structure, Auger recombination threatens to provide another pathway for efficiency roll-off. Auger recombination is a three-particle non-radiative process in which an electron and a hole recombine and their energy is transferred to a third free carrier in the form of kinetic energy. Because an Auger recombination event requires three charge carriers, the rate of Auger recombination scales with n^3, where n is the density of charge carriers, and consequently recombination is predominantly monomolecular (rate $\propto n$) or bimolecular (rate $\propto n^2$) at low carrier concentrations, while Auger may become dominant at high n. The carrier densities at which each recombination pathway becomes dominant is highly material-dependent, and it remains an open question whether Auger recombination may impede electrically pumped lasing in perovskites. Thus far, reports of Auger processes in perovskite films and LEDs have yielded mixed conclusions.

Zou *et al.* claimed that Auger recombination was responsible for EQE roll-off at J < 100 mA/cm^2 in quasi-2D perovskite LEDs based on $FAPbI_3$ [FA = formamidinium, $CH(NH_2)_2^+$].[44] By simultaneously measuring the EQE and PLQE during a voltage sweep [see Fig. 4(a)] and observing concurrent roll-off of both, the authors determined that a luminescence quenching effect was primarily responsible for EQE roll-off (rather than, e.g., charge imbalance). As shown in Figs. 7(a) and 7(b), PLQE and TRPL were measured in the quasi-2D perovskite films at varied excitation fluence, and both the PLQE and the PL lifetime were found to decrease above a fluence of ~30 nJ/cm^2, corresponding to a carrier density of $n \sim 3 \times 10^{15}$ cm^{-3}. Richter *et al.* previously determined the rate constants for each recombination pathway in $MAPbI_3$ perovskite using transient absorption (TA) measurements at varied excitation fluence.[51] Figure 7(c) shows the trend in carrier decay rate (dn/dt) vs carrier density (n) extracted from TA measurements, from which it is clear that Auger (3rd order) recombination only becomes significant above ~10^{18} cm^{-3}. Zou *et al.* proposed that the onset of Auger recombination at low carrier density may be due to an effect specific

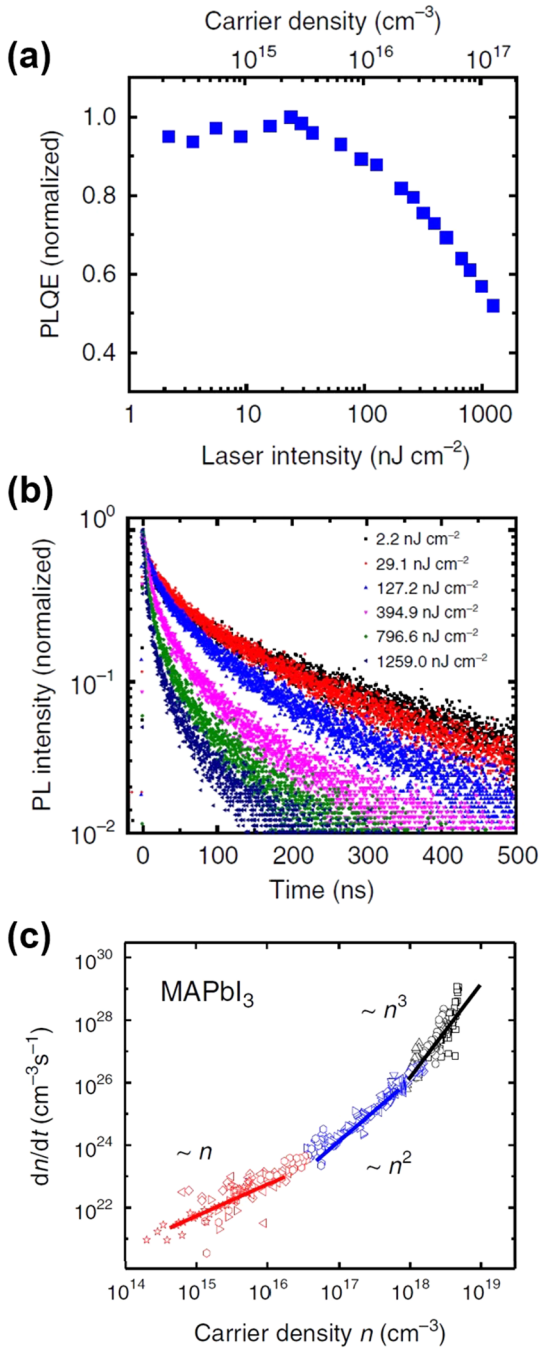

FIG. 7. (a) Normalized PLQE of a quasi-2D perovskite film at varied pulsed laser intensity, with computed carrier density shown above the plot. (b) TRPL measured in the same film at various pulsed laser intensities (see legend), revealing similar trends in the PLQE and PL lifetime. Reproduced with permission from Zou *et al.*, Nat. Commun. **9**, 608 (2018). Copyright 2018 Springer Nature. (c) Carrier decay rates in $MAPbI_3$ extracted from TA measurements at varied excitation fluence. The dominant recombination mechanism is labeled for each range of carrier densities (i.e., monomolecular ~ n, bimolecular ~ n^2, and Auger ~ n^3) based on the slope of dn/dt vs n. Reproduced with permission from Richter *et al.*, Nat. Commun. **7**, 013941 (2016). Copyright 2016 Springer Nature.

to their quasi-2D perovskite, such as accumulation of charge carriers in low-bandgap regions.[44]

Kim *et al.* also investigated the potential for Auger recombination in $MAPbI_3$ LEDs at high current density.[26] As shown in Figs. 8(a) and 8(b), TRPL measurements were performed on a $MAPbI_3$ LED during 1.5 μs electrical pulses with current density varied from 0 to 156 A/cm^2 (TRPL measured at the front end of the pulse to minimize effects of Joule heating). The PL lifetime remains unchanged as the current density increases from 0 to 156 A/cm^2, which suggests that carrier density-dependent quenching mechanisms such as Auger recombination are not at play. However, electrically pumped lasing may require another order of magnitude or more in current density, and the estimated threshold carrier density $n_{th} \sim 8 \times 10^{17}$ cm^{-3} is near the carrier density at which Auger is predicted to become significant.

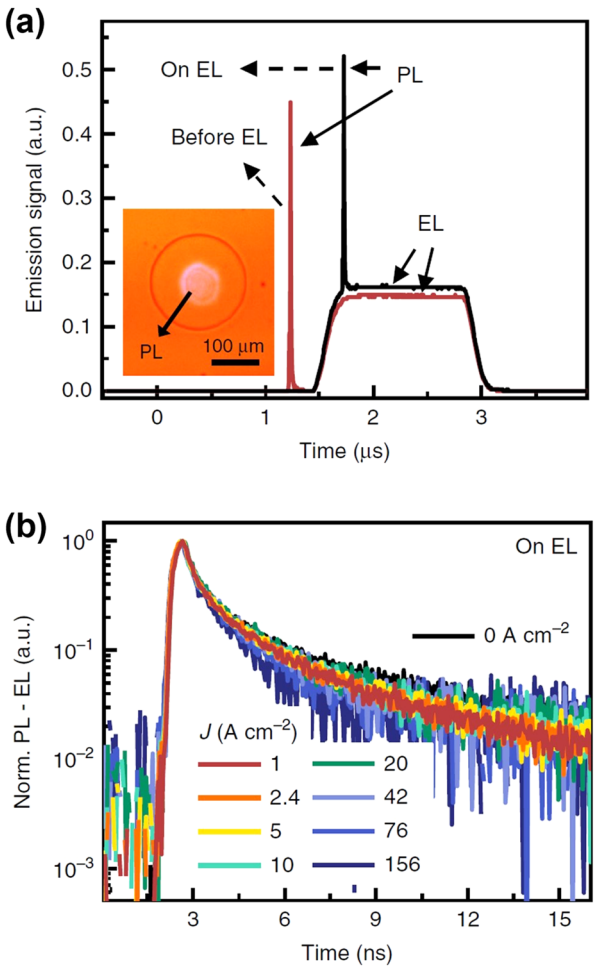

FIG. 8. (a) Emission from a $MAPbI_3$ LED subject to an optical pulse (20 ps, 10.7 μJ/cm^2) just before or after the onset of a 1.5 μs electrical pulse (J = 45 A/cm^2). The inset shows the location of the optical excitation within the device area. (b) TRPL signal measured just after the onset of an electrical pulse [as depicted in (a)], with current density varied from 0 to 156 A/cm^2. Reproduced with permission from Kim *et al.*, Nat. Commun. **9**, 4893 (2018). Copyright 2018 Springer Nature.

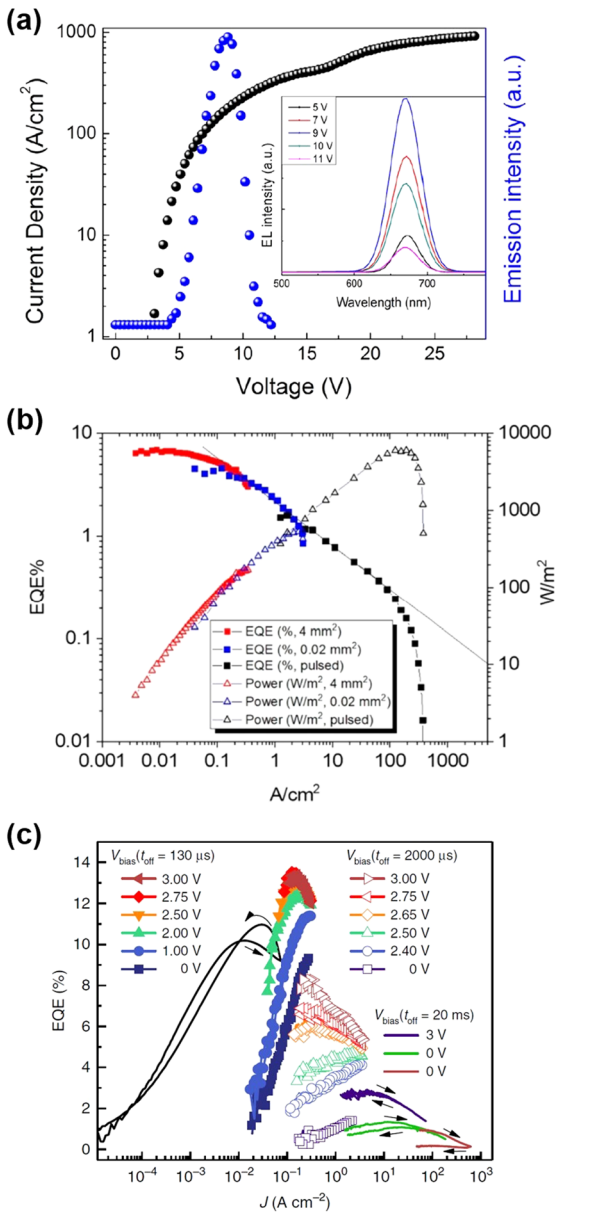

FIG. 9. (a) DC current density (black) and emission intensity (blue) vs applied voltage for a small-area (0.1 mm × 0.1 mm) $CsSnBr_3$ LED. The inset shows emission profile at different applied voltages. Reproduced with permission from Yuan *et al.*, Phys. Status Solidi RRL **12**, 1800090 (2018). Copyright 2018 Wiley-VCH. (b) EQE (filled symbols) and emitted power (hollow symbols) from quasi-2D perovskite LEDs as a function of current density. Large-area (red) and small-area (blue) devices were characterized in DC operation, and a small-area device was measured under pulsed current (black, pulse width of ~500 ns). In pulsed mode, only relative EQE was measured, and values were scaled to align with DC measurements. Reprinted with permission from Leyden *et al.*, ACS Photonics **6**, 460 (2019). Copyright 2019 American Chemical Society. (c) EQE vs current density in a small-area $MAPbI_3$ LED under DC (black lines) and pulsed (pulse width of 70 μs, 15 μs, and 2 μs for filled symbols, hollow symbols, and colored lines, respectively) excitation. Time between pulses (t_{off}) and background voltage bias (V_{bias}) are labeled for each set of traces. Reproduced with permission from Kim *et al.*, Nat. Commun. **9**, 4893 (2018). Copyright 2018 Springer Nature.

III. PEROVSKITE LEDS OPERATED AT $J > 100$ A/cm^2

There have so far been few attempts to reach current densities relevant to electrically pumped lasing (at least hundreds of A/cm^2) in perovskite LEDs. In each case, the LEDs under investigation degraded at $J < 1$ kA/cm^2, despite efforts to alleviate Joule heating.

In one report, a small-area (0.1 mm × 0.1 mm) LED featuring an evaporated $CsSnBr_3$ emissive layer was subjected to current densities up to 915 A/cm^2 before undergoing permanent degradation, likely due to Joule heating.[52] Figure 9(a) shows the J–V characteristic of the device as well as EL intensity, with luminescence profiles at various bias conditions shown in the inset. While 915 A/cm^2 is predicted to be near the current density required for lasing, the EL begins to roll off at around 8 V and is completely quenched by 13 V, likely due to a combination of heating, charge imbalance, and field-related effects, though the exact causes were not investigated. In another work, quasi-2D perovskite LEDs were operated at current densities up to nearly 400 A/cm^2, taking advantage of both reduced device area (0.02 mm^2) and short excitation pulses (~500 ns) to maximize EL at high currents.[53] As seen in Fig. 9(b), both reduction of device area and the switch from continuous to pulsed operation extend the range of current densities before roll-off accelerates severely, though EQE decreases steadily beginning at ~20 mA/cm^2. The cause of roll-off in this case is again likely a combination of multiple effects dominated by Joule heating. Kim *et al.* observed small-area $MAPbI_3$ LEDs (200 μm diameter) under short (down to 2 μs) electrical pulses with current densities up to 620 A/cm^2 (Ref. 26). Figure 9(c) shows that EQE is heavily influenced by the pulsing scheme and background DC bias, which primarily impact Joule heating and mobile ion redistribution, respectively. Roll-off was carefully investigated and attributed to heating and charge carrier imbalance, while Auger recombination was ruled out, as discussed in detail in Sec. II D. The peak EQE–J product measured by Kim *et al.* was 1.3 A/cm^2, well below the predicted lasing threshold value, 62 A/cm^2 (Ref. 26).

IV. CONCLUSION

While the perovskite LED structure remains a promising candidate for electrically driven lasing in a non-epitaxial semiconductor, substantial obstacles must be surmounted to reach this goal. The operational stability of perovskite LEDs and their EQEs at high current densities must be enhanced if the predicted threshold EQE–J product of 62 A/cm^2 is to be achieved. The primary challenges identified in the literature result from Joule heating, charge injection imbalance, electric fields in the emissive layer, and Auger recombination. Of these, Joule heating appears to be the most deleterious, preventing LEDs from reaching current densities greater than a few hundred A/cm^2 without total emission quenching. Further improvement of heat dissipation and reduction of pulse width should relieve heat-driven roll-off and degradation, although it may still be necessary to lower the environmental temperature for lasing threshold to be reached. Adjustments to device architecture and electrical drive scheme have proven effective in reducing problems due to charge imbalance and electric fields, respectively, while Auger recombination may be difficult to address if it becomes significant at $J > 1$ kA/cm^2. Ultimately, it remains to be seen whether electrically driven lasing in perovskites is achievable, though demonstrations of high-efficiency LEDs and optically pumped lasing in LED structures suggest this goal may be within reach.

ACKNOWLEDGMENTS

We thank Dr. Nakita Noel for valuable conversations and input. We acknowledge support for this work from the Air Force Office of Scientific Research under Award No. FA9550-18-1-0037. W.B.G. acknowledges support from the National Science Foundation Graduate Research Fellowship Program under Grant No. DGE-1656466.

REFERENCES

[1] M. A. Green, A. Ho-Baillie, and H. J. Snaith, Nat. Photonics **8**, 506 (2014).
[2] S. Il Seok, M. Grätzel, and N. G. Park, Small **14**, 1704177 (2018).
[3] L. N. Quan, B. P. Rand, R. H. Friend, S. G. Mhaisalkar, T. W. Lee, and E. H. Sargent, Chem. Rev. **119**, 7444 (2019).
[4] Q. Zhang, R. Su, W. Du, X. Liu, L. Zhao, S. T. Ha, and Q. Xiong, Small Methods **1**, 1700163 (2017).
[5] Q. Wei, X. Li, C. Liang, Z. Zhang, J. Guo, G. Hong, G. Xing, and W. Huang, Adv. Opt. Mater. **7**, 1900080 (2019).
[6] F. Deschler, M. Price, S. Pathak, L. E. Klintberg, D. D. Jarausch, R. Higler, S. Hüttner, T. Leijtens, S. D. Stranks, H. J. Snaith, M. Atatüre, R. T. Phillips, and R. H. Friend, J. Phys. Chem. Lett. **5**, 1421 (2014).
[7] B. R. Sutherland, S. Hoogland, M. M. Adachi, C. T. O. Wong, and E. H. Sargent, ACS Nano **8**, 10947 (2014).
[8] B. Tang, H. Dong, L. Sun, W. Zheng, Q. Wang, F. Sun, X. Jiang, A. Pan, and L. Zhang, ACS Nano **11**, 10681 (2017).
[9] Q. Zhang, S. T. Ha, X. Liu, T. C. Sum, and Q. Xiong, Nano Lett. **14**, 5995 (2014).
[10] H. Zhu, Y. Fu, F. Meng, X. Wu, Z. Gong, Q. Ding, M. V. Gustafsson, M. T. Trinh, S. Jin, and X. Y. Zhu, Nat. Mater. **14**, 636 (2015).
[11] N. Pourdavoud, T. Haeger, A. Mayer, P. J. Cegielski, A. L. Giesecke, R. Heiderhoff, S. Olthof, S. Zaefferer, I. Shutsko, A. Henkel, D. Becker-Koch, M. Stein, M. Cehovski, O. Charfi, H. H. Johannes, D. Rogalla, M. C. Lemme, M. Koch, Y. Vaynzof, K. Meerholz, W. Kowalsky, H. C. Scheer, P. Görrn, and T. Riedl, Adv. Mater. **31**, 1903717 (2019).
[12] Y. Jia, R. A. Kerner, A. J. Grede, A. N. Brigeman, B. P. Rand, and N. C. Giebink, Nano Lett. **16**, 4624 (2016).
[13] P. Brenner, M. Stulz, D. Kapp, T. Abzieher, U. W. Paetzold, A. Quintilla, I. A. Howard, H. Kalt, and U. Lemmer, Appl. Phys. Lett. **109**, 141106 (2016).
[14] K. Roh, L. Zhao, W. B. Gunnarsson, Z. Xiao, Y. Jia, N. C. Giebink, and B. P. Rand, ACS Photonics **6**, 3331 (2019).
[15] H. Kim, K. Roh, J. P. Murphy, L. Zhao, W. B. Gunnarsson, E. Longhi, S. Barlow, S. R. Marder, B. P. Rand, and N. C. Giebink, Adv. Opt. Mater. **8**, 1901297 (2019).
[16] Y. Jia, R. A. Kerner, A. J. Grede, B. P. Rand, and N. C. Giebink, Adv. Opt. Mater. **8**, 1901514 (2019).
[17] Y. Jia, R. A. Kerner, A. J. Grede, B. P. Rand, and N. C. Giebink, Nat. Photonics **11**, 784 (2017).
[18] P. Brenner, O. Bar-On, M. Jakoby, I. Allegro, B. S. Richards, U. W. Paetzold, I. A. Howard, J. Scheuer, and U. Lemmer, Nat. Commun. **10**, 988 (2019).
[19] L. N. Quan, F. P. García de Arquer, R. P. Sabatini, and E. H. Sargent, Adv. Mater. **30**, 1801996 (2018).
[20] K. Lin, J. Xing, L. N. Quan, F. P. G. de Arquer, X. Gong, J. Lu, L. Xie, W. Zhao, D. Zhang, C. Yan, W. Li, X. Liu, Y. Lu, J. Kirman, E. H. Sargent, Q. Xiong, and Z. Wei, Nature **562**, 245 (2018).
[21] B. Zhao, S. Bai, V. Kim, R. Lamboll, R. Shivanna, F. Auras, J. M. Richter, L. Yang, L. Dai, M. Alsari, X. J. She, L. Liang, J. Zhang, S. Lilliu, P. Gao, H. J. Snaith, J. Wang, N. C. Greenham, R. H. Friend, and D. Di, Nat. Photonics **12**, 783 (2018).

[22]Y. Cao, N. Wang, H. Tian, J. Guo, Y. Wei, H. Chen, Y. Miao, W. Zou, K. Pan, Y. He, H. Cao, Y. Ke, M. Xu, Y. Wang, M. Yang, K. Du, Z. Fu, D. Kong, D. Dai, Y. Jin, G. Li, H. Li, Q. Peng, J. Wang, and W. Huang, Nature **562**, 249 (2018).
[23]T. Chiba, Y. Hayashi, H. Ebe, K. Hoshi, J. Sato, S. Sato, Y. J. Pu, S. Ohisa, and J. Kido, Nat. Photonics **12**, 681 (2018).
[24]Z. Xiao, R. A. Kerner, L. Zhao, N. L. Tran, K. M. Lee, T. W. Koh, G. D. Scholes, and B. P. Rand, Nat. Photonics **11**, 108 (2017).
[25]M. Yuan, L. N. Quan, R. Comin, G. Walters, R. Sabatini, O. Voznyy, S. Hoogland, Y. Zhao, E. M. Beauregard, P. Kanjanaboos, Z. Lu, D. H. Kim, and E. H. Sargent, Nat. Nanotechnol. **11**, 872 (2016).
[26]H. Kim, L. Zhao, J. S. Price, A. J. Grede, K. Roh, A. N. Brigeman, M. Lopez, B. P. Rand, and N. C. Giebink, Nat. Commun. **9**, 4893 (2018).
[27]M. Yang, N. Wang, S. Zhang, W. Zou, Y. He, Y. Wei, M. Xu, J. Wang, and W. Huang, J. Phys. Chem. Lett. **9**, 2038 (2018).
[28]L. Zhao, Y. W. Yeh, N. L. Tran, F. Wu, Z. Xiao, R. A. Kerner, Y. L. Lin, G. D. Scholes, N. Yao, and B. P. Rand, ACS Nano **11**, 3957 (2017).
[29]L. Zhao, J. Gao, Y. H. L. Lin, Y. W. Yeh, K. M. Lee, N. Yao, Y. L. Loo, and B. P. Rand, Adv. Mater. **29**, 1605317 (2017).
[30]L. Zhao, K. M. Lee, K. Roh, S. U. Z. Khan, and B. P. Rand, Adv. Mater. **31**, 1805836 (2019).
[31]V. Prakasam, D. Tordera, H. J. Bolink, and G. Gelinck, Adv. Opt. Mater. **7**, 1900902 (2019).
[32]Z. Shi, S. Li, Y. Li, H. Ji, X. Li, D. Wu, T. Xu, Y. Chen, Y. Tian, Y. Zhang, C. Shan, and G. Du, ACS Nano **12**, 1462 (2018).
[33]R. L. Milot, G. E. Eperon, H. J. Snaith, M. B. Johnston, and L. M. Herz, Adv. Funct. Mater. **25**, 6218 (2015).
[34]Y. Zou and R. J. Holmes, Adv. Energy Mater. **6**, 1501994 (2016).
[35]Y. Yuan and J. Huang, Acc. Chem. Res. **49**, 286 (2016).
[36]O. Svelto, *Principles of Lasers*, 5th ed. (Springer, 2010).
[37]A. Pisoni, J. Jaćimović, O. S. Barišić, M. Spina, R. Gaál, L. Forró, and E. Horváth, J. Phys. Chem. Lett. **5**, 2488 (2014).
[38]X. Qian, X. Gu, and R. Yang, Appl. Phys. Lett. **108**, 063902 (2016).
[39]N. Kim, B. Domercq, S. Yoo, A. Christensen, B. Kippelen, and S. Graham, Appl. Phys. Lett. **87**, 241908 (2005).
[40]D. Kasemann, R. Brückner, H. Fröb, and K. Leo, Phys. Rev. B **84**, 115208 (2011).
[41]T. Matsushima, H. Sasabe, and C. Adachi, Appl. Phys. Lett. **88**, 033508 (2006).
[42]H. Nakanotani, T. Oyamada, Y. Kawamura, H. Sasabe, and C. Adachi, Jpn. J. Appl. Phys., Part 1 **44**, 3659 (2005).
[43]M. Xu, Q. Peng, W. Zou, L. Gu, L. Xu, L. Cheng, Y. He, M. Yang, N. Wang, W. Huang, and J. Wang, Appl. Phys. Lett. **115**, 041102 (2019).
[44]W. Zou, R. Li, S. Zhang, Y. Liu, N. Wang, Y. Cao, Y. Miao, M. Xu, Q. Guo, D. Di, L. Zhang, C. Yi, F. Gao, R. H. Friend, J. Wang, and W. Huang, Nat. Commun. **9**, 608 (2018).
[45]A. Fakharuddin, W. Qiu, G. Croes, A. Devižis, R. Gegevičius, A. Vakhnin, C. Rolin, J. Genoe, R. Gehlhaar, A. Kadashchuk, V. Gulbinas, and P. Heremans, Adv. Funct. Mater. **29**, 1904101 (2019).
[46]C. Eames, J. M. Frost, P. R. F. Barnes, B. C. O'Regan, A. Walsh, and M. S. Islam, Nat. Commun. **6**, 7497 (2015).
[47]F. Yuan, Z. Wu, H. Dong, B. Xia, J. Xi, S. Ning, L. Ma, and X. Hou, Appl. Phys. Lett. **107**, 261106 (2015).
[48]N. Ahn, K. Kwak, M. S. Jang, H. Yoon, B. Y. Lee, J. K. Lee, P. V. Pikhitsa, J. Byun, and M. Choi, Nat. Commun. **7**, 13422 (2016).
[49]R. L. Z. Hoye, M. R. Chua, K. P. Musselman, G. Li, M. L. Lai, Z. K. Tan, N. C. Greenham, J. L. MacManus-Driscoll, R. H. Friend, and D. Credgington, Adv. Mater. **27**, 1414 (2015).
[50]J. Wang, N. Wang, Y. Jin, J. Si, Z. K. Tan, H. Du, L. Cheng, X. Dai, S. Bai, H. He, Z. Ye, M. L. Lai, R. H. Friend, and W. Huang, Adv. Mater. **27**, 2311 (2015).
[51]J. M. Richter, M. Abdi-Jalebi, A. Sadhanala, M. Tabachnyk, J. P. H. Rivett, L. M. Pazos-Outón, K. C. Gödel, M. Price, F. Deschler, and R. H. Friend, Nat. Commun. **7**, 13941 (2016).
[52]F. Yuan, J. Xi, H. Dong, K. Xi, W. Zhang, C. Ran, B. Jiao, X. Hou, A. K. Y. Jen, and Z. Wu, Phys. Status Solidi RRL **12**, 1800090 (2018).
[53]M. R. Leyden, S. Terakawa, T. Matsushima, S. Ruan, K. Goushi, M. Auffray, A. S. D. Sandanayaka, C. Qin, F. Bencheikh, and C. Adachi, ACS Photonics **6**, 460 (2019).